

Nonlinear modeling of flat-plate structures using grid beam elements

Ying Tian*¹, Jianwei Chen², Aly Said¹ and Jian Zhao³

¹*Department of Civil and Environmental Engineering and Construction,
University of Nevada Las Vegas, Las Vegas, USA*

²*College of Civil and Architectural Engineering, Hebei United University, Tangshan, China*

³*Department of Civil Engineering and Mechanics, University of Wisconsin – Milwaukee, Milwaukee, USA*

(Received December 8, 2011, Revised May 9, 2012, Accepted May 18, 2012)

Abstract. This paper presents a simplified grid beam model for simulating the nonlinear response of reinforced concrete flat-plate structures. The beam elements are defined with nonlinear behavior for bending moment and torsion. The flexural stiffness and torsional strength of the beam elements are defined based on experimental data to implicitly account for slab two-way bending effects. A failure criterion that considers the interaction between the punching strength and slab flexural behavior is incorporated in the model. The effects of bond-slip of slab reinforcement on connection stiffness are examined. The proposed grid beam model is validated by simulating large-scale tests of slab-column connections subjected to concentric gravity loading and unbalanced moment. This study also determines the critical parameters for a hysteretic model used to simulate flat-plates subjected to cyclic lateral loading.

Keywords: cyclic loading; flat-plate; grid model; hysteretic behavior; punching failure; slab-column connection.

1. Introduction

Reinforced concrete flat-plates are structural systems containing slabs supported directly on columns without using beams. Flat-plates are widely used for the structures with light gravity loads such as residential and office buildings in both non-seismic and seismic regions. Simulating the nonlinear response of flat-plate structures is challenging because of the complex state of stresses in the slab nearby the supporting columns and the material nonlinearity caused by concrete cracking and steel yielding. Appropriately modeling the nonlinear behavior of slab-column connections is the key to capture the overall response of the entire flat-plate system. Simplified modeling approaches including the equivalent frame method and the effective beam width method, have been proposed for the analyses of flat-plates (Akiyama and Hawkins 1984, Luo *et al.* 1994, Robertson 1997, Dovich and Wight 2005, Tian *et al.* 2009, Kang *et al.* 2009). These methods were developed only for flat-plates where the nonlinear behavior is dominated by seismic lateral loads. Additionally, both methods are two-dimensional as a structure needs to be idealized into a set of parallel planar frames, thereby limiting their capability to capture the three-dimensional load redistribution that is critical for flat-plates subjected to other loading conditions.

* Corresponding author, Ph.D., E-mail: ying.tian@unlv.edu

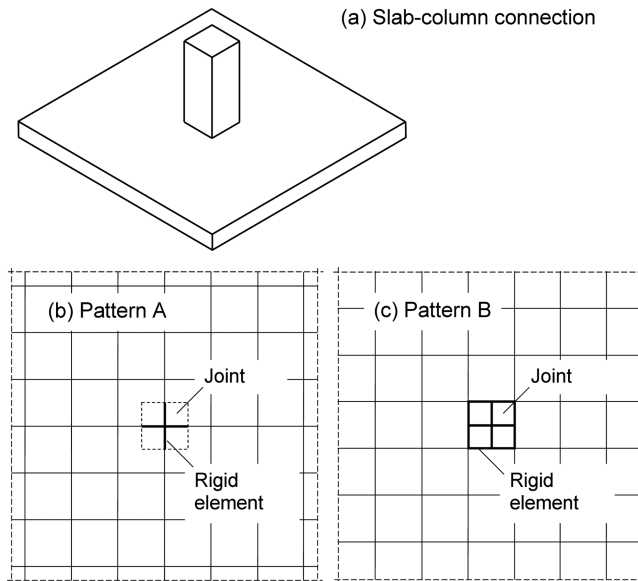


Fig. 1 Two grid beam patterns for modeling reinforced concrete flat-plates

Compared with the equivalent frame method and the effective beam width method, grid beam model requires more computational efforts but is suitable for the analyses of flat-plates with irregular floor plans or under complex loading conditions. In this approach, the slab is idealized as interconnected beams, as shown in Fig. 1. Two grid beam patterns have been studied. Sheu and Hawkins (1980) formulated a grid model similar to that shown in Fig. 1(b) for slab-column connections under monotonic and cyclic lateral loading. The slab-column joint was assumed with zero dimension and thus no rigid element representing the joint zone was considered. Using the grid pattern shown in Fig. 1(b), Coronelli (2010) developed a model capable of predicting the ultimate punching failure of connections under concentric gravity and monotonic lateral loading. It is noteworthy that, for a lightly reinforced slab-column connection under symmetric gravity loading, this grid pattern may predict a very local flexural failure mechanism rather than that corresponding to the expected slab yield-line pattern. Fig. 1(c) shows another grid beam pattern used by Morrison *et al.* (1983) for modeling flat-plates under monotonic lateral loading. The model, however, is unsuitable for flat-plates under gravity loading. In all these aforementioned studies, bending moment, shear and torsion in the grid beams are decoupled except that the torsional strength may be defined as a function of gravity shear. However, these studies varied considerably in formulating the flexural stiffness, bond-slip behavior, torsional stiffness and strength, and failure criterion.

This study focuses on using grid beam elements to simulate the nonlinear behavior of flat-plates with square columns and low-to-moderate slab tensile reinforcement ratios typically used in practice. The primary objective is to develop a grid beam model applicable to the flat-plates subjected to concentric gravity loading and those under unbalanced moment caused by lateral loads or unevenly distributed gravity loads. To predict the failure of slab-column connections, the new punching failure criterion developed by Muttoni (2008) is incorporated in the suggested model and examined. The study also determines the parameters needed to define a hysteretic model for slab-column connections subjected to cyclic lateral loading. Thirteen tests of isolated slab-column connections under a variety of loading conditions are simulated to calibrate and validate the key modeling parameters.

2. Model description

2.1 General

When a slab-column connection transfers unbalanced moment, the slab develops torsion (T) at the side faces of column, as shown in Fig. 2. Different from the grid pattern shown in Fig. 1(b), two beam elements frame into the column at each face in the grid pattern shown in Fig. 1(c). The torsion at each side face is resisted by not only the torque (T_1 and T_2 in Fig. 2) but also the force couple formed by the vertical shears ($V_{T,1}$ and $V_{T,2}$) in the two beam elements. Accordingly, the portion of unbalanced moment that must be carried by torsion in each beam element is reduced, which minimizes the influence of uncertainty involved in defining torsional properties. This grid pattern is therefore adopted in this study to simulate the nonlinear response of flat-plates with square columns. All the beam elements nearby the column have an identical length equal to column size, leading to a square grid beam pattern. The beams are defined with a depth equal to the slab thickness h and a width equal to the grid size b . The slab-column joint is represented in the model by rigid beam elements. The columns are modeled as beam-column elements connected with joint center. Tests (Elstner and Hognestad 1956, Tian *et al.* 2008, Guadalini *et al.* 2009) indicated that the deformation of a slab-column connection at failure is caused primarily by excessive slab rotation at column due to localized crack opening and reinforcement yielding. Thus, nonlinear behavior is defined only for principal bending moment and torsion of grid beams, whereas all other actions are assumed to be elastic.

2.2 Nonlinear model for flexure

A tri-linear moment-curvature relationship shown in Fig. 3(a) is considered for the principal moment in grid beams under monotonic loading. Three characteristic loading stages are defined in this model: concrete cracking, reinforcement yielding and concrete crushing. Following Coronelli's suggestion (2010), the initial flexural stiffness of a grid beam (K_F) is defined as

$$K_F = 0.5E_cI_g \tag{1}$$

where E_c is the Young's modulus of concrete and I_g is the moment of inertia of beam. The concrete modulus of rupture for evaluating cracking moment M_{cr} is also reduced by half to account for (1)

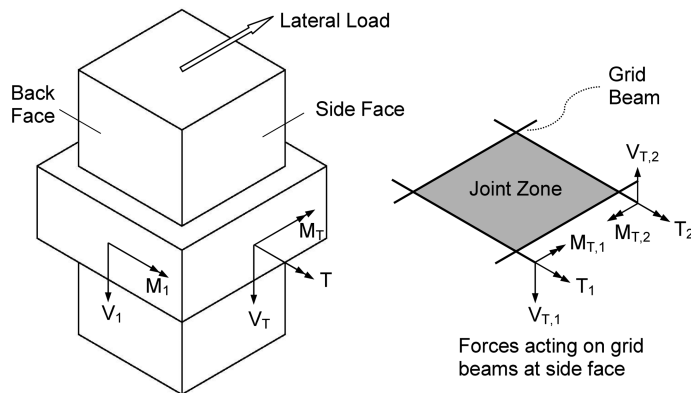


Fig. 2 Forces in grid beams resisting torsion

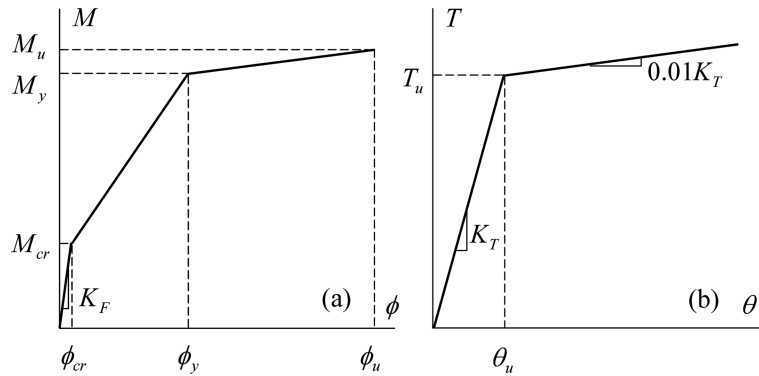


Fig. 3 Nonlinear model for grid beams: (a) flexure and (b) torsion

the reduced stress concentration at each side of slab-column joint caused by using two beam elements that have a total width twice of the column dimension and (2) the initial tensile stress due to restrained concrete shrinkage prior to applying any loads.

The principal bending moment and curvature of a grid beam at the yielding of tensile reinforcement and at the ultimate are defined based on the slab within a width of b . Because reinforcing bars resist bending one-dimensionally, it is assumed that slab two-way bending has little effect on the yield moment M_y and ultimate moment M_u . Thus, they are determined using conventional procedures for one-way slabs. However, the actually existing two-way bending especially the presence of torsion may cause the post-cracking stiffness of slab significantly lower from that of a one-way slab. For this reason, a correction factor of γ is considered to incorporate the two-way bending effects on slab deformation. The yield curvature ϕ_y is given as

$$\phi_y = \gamma\phi_{y,0} \quad (2)$$

where $\phi_{y,0}$ is the yield curvature evaluated using a section analysis of a beam based on plane section assumption. The appropriate value of γ is to be calibrated in this study from test data, as discussed later.

The ultimate curvature, ϕ_u is also likely affected by slab two-way bending; however the definition for ϕ_u is less critical than that for yield curvature. This is because the yield moment is close to the ultimate moment for slabs with typical reinforcement ratios and slab-column connections generally failed in punching before crushing of slab concrete could be observed. ϕ_u is used in the model mainly to control the post-yielding flexural stiffness of grid beams. For simplicity, a concrete crushing strain of 0.004 is used to determine the ultimate curvature.

2.3 Nonlinear model for torsion

The actual behavior of torsion in slab near column is complex and it is difficult to isolate the effects of other actions on torsion based on the test data of slabs. For simplicity, a bilinear relationship shown in Fig. 3(b) is assumed for the torque versus twist angle response under monotonic loading and applied to all the grid beam elements. Tests indicated (Tian *et al.* 2008) that torsional cracking occurred after flexural cracking. Additionally, the Poisson's ratio of slab concrete approaches zero as the slab is fully cracked (Park and Gamble 2000). Based on rigidity equivalence between a continuous

plate and the substituting grid beams, Yettram and Husain (1965) derived that, if Poisson's ratio is equal to zero, the elastic torsional stiffness of beams with a square grid pattern is identical to their flexural stiffness. Thus, the torsional stiffness K_T of beam elements is defined in this study as

$$K_T = K_F = 0.5E_cI_g \quad (3)$$

Compared with using polar moment of inertia and shear modulus to define K_T , the use of Eq. (3) eliminates the sensitivity of torsional stiffness (relative to flexural stiffness) to mesh size.

Dimensionless interaction relationship between torsion and shear was considered by Sheu and Hawkins (1980) and Coronelli (2010) to define the torsional strength of beams connected directly with slab-column joint. Such an interaction was developed for flat-plates subjected to lateral loading and shear must be assumed as constant. No torsion-shear interaction was assumed for the grid beams elsewhere. Because the bending moment, shear and torsion may keep changing when a slab is loaded under other loading conditions, this type of interaction is not incorporated in this study. Instead, the reduction in torsional capacity of grid beams due to bending is considered implicitly. Incorporating a simple interaction between flexure and torsion, the torsional strength of a grid beam is limited to $T_u = \lambda T_{cr}$, where T_{cr} is the pure torsional resistance at cracking of the grid beam and λ is a strength reduction factor to be calibrated from test data. Eq. (4), developed by Hsu (1968) for beams without shear reinforcement, is adopted to define T_{cr} . The tests by Kanoh and Yoshizaki (1979) indicated that, because of slab flexural reinforcement, torsional cracking in slab did not lead to an immediate drop of torsional strength and the torsional behavior is fairly ductile. Thus, no strength degradation is assumed following the reach of T_u . To ensure convergence in an analysis, $0.01K_T$ is assumed for the torsional stiffness beyond T_u .

$$T_{cr} = 0.217y(x^2 + 6450)(\sqrt[3]{f'_c}) \quad (\text{units: mm and MPa}) \quad (4)$$

where x and y are the smaller and the larger dimension of grid beam cross section, respectively. For a flat-plate with typical dimensions of column and slab, x and y are equal to slab thickness and column size, respectively.

2.4 Failure criterion

The failure of flat-plates is normally announced by the punching failure of slabs near the columns. The failure criterion suggested by Muttoni (2008) based on a critical shear crack theory is adopted to detect punching failure in the analyses of flat-plate subjected to monotonic loading. It assumes that the opening of critical inclined cracks reduces the ability of concrete in compression to resist punching failure. The width of critical crack was assumed to be proportional to θd , where θ is the rotation of slab outside the critical crack and d is slab effective depth. According to this failure condition, the punching strength V_u for slab at one side of the slab-column joint is given as a function of slab rotation at failure θ_u as

$$\frac{V_u}{b_0 d \sqrt{f'_c}} = \frac{3/4}{1 + 15 \frac{\theta_u d}{d_{g0} + d_g}} \quad (\text{units: mm and MPa}) \quad (5)$$

where b_0 is the perimeter of shear critical section taken $d/2$ from the column face, d_g is the maximum size of the aggregate, and d_{g0} is a reference aggregate size equal to 16 mm. The advantage of this failure criterion is that the punching shear strength of slabs is correlated to their flexural

behavior, a property that has been repeatedly observed in tests. Eq. (5) implies that slab rotation capacity increases as the punching strength decreases. The intersection of the V_u vs. θ_u interaction defined by Eq. (5) and the slab shear vs. rotation response determined from analysis predicts the slab punching strength as well as failure rotation.

2.5 Hysteretic behavior for flexure and torsion

Due to slab crack opening and closing, a slab-column connection under lateral loading reversals is characterized by severe pinching of load-deformation loops. When simulating the seismic behavior of flat-plates using grid beams, the hysteretic property needs to be effectively defined to avoid overestimating the energy dissipated by slab-column connections. For this purpose, the hysteretic model considered by Elwood (2002) for general reinforced concrete structural components (Fig. 4) is adopted as a platform to define the cyclic response of flexure and torsion in grid beams. The ordinate S in Fig. 4 expresses principal moment (or torque) and the abscissa e represents curvature (or twist angle). The monotonic loading response shown in Fig. 3 defines the response envelop. To apply this hysteretic model, at least three parameters, p_x , p_y and β (all with a value less than 1) need to be defined. The factor β is associated with unloading stiffness degradation; the factors p_x and p_y are used to simulate the pinching effects for curvature (or twist angle) and moment (or torque) during reloading, respectively. $p_x=0.5$, $p_y=0.2$ and $\beta=0.5$ were used by Kang *et al.* (2009) in the equivalent frame model for flat-plates. An additional parameter, γ_1 , is employed in the present study. This parameter considers the damage related to strain energy and is used to define the effects of loading intensity (the number of loading cycles at a drift level) on stiffness degradation during reloading. The same set of modeling parameters are used for both principal moment and torsion. The values of these parameters, as discussed later, will be calibrated from the test of a slab-column connection subjected to cyclic lateral loading. It is noted that, when the hysteretic model is used for bending moment, the point at elastic limit S_1 is defined at flexural cracking rather than reinforcement yielding. This is because pinching due to slab stiffness degradation during unloading and reloading occurs even prior to yielding in slab-column connections subjected to lateral loading (Tian 2007).

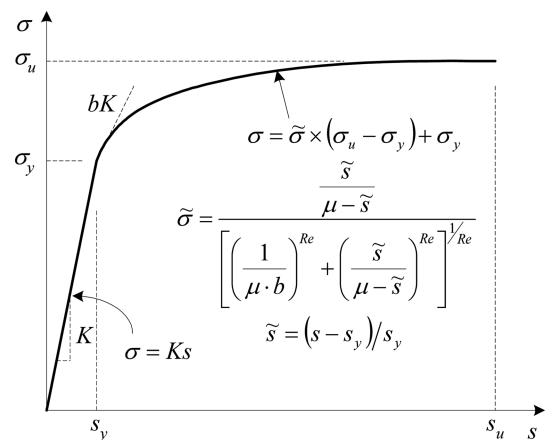
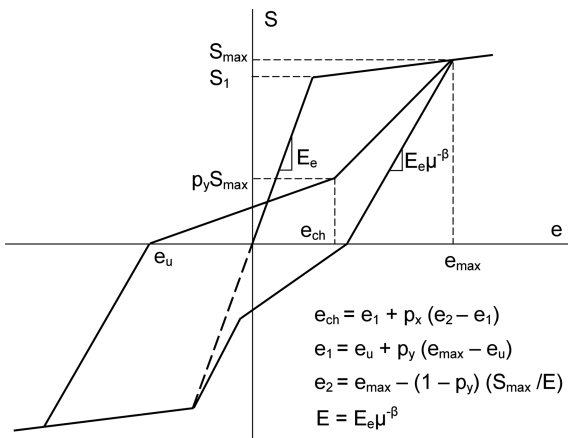


Fig. 4 Hysteretic model (Elwood 2002) for flexure and torsion in grid beams Fig. 5 Bar stress versus loaded-end slip response (Zhao and Sritharan 2007)

2.6 Modeling for bond-slip

The effects of bond-slip of slab flexural reinforcement are examined in this study. Due to its simplicity, the bond-slip model proposed by Zhao and Sritharan (2007) and validated by experimental data of columns is adopted. This model is applicable for fully anchored reinforcing bars, which is the case for slab tensile reinforcement at column resisting negative bending moment. As shown in Fig. 5, bond slip under monotonic loading is defined through the relationship between stress, σ , and slip, s , of a bar at its end connecting with column. In this formulation, bar slip at yielding, s_y , is defined by Eq. (6) and the bar slip at fracture, s_u , is estimated as $30\sim 40s_y$. A linear σ - s response is assumed prior to bar yielding, whereas a curvilinear relationship is assumed between the reaches of s_y and s_u .

$$s_y = 2.54 \left(\frac{d_b f_y}{8437 \sqrt{f'_c}} (2\alpha + 1) \right)^{1/\alpha} + 0.34 \quad (\text{units: mm and MPa}) \quad (6)$$

where d_b is bar diameter and α can be taken as 0.4 (FIB 2000).

3. Calibration and validation of modeling parameters

3.1 Simulating slab-column connections using OpenSees

Tests conducted by Elstner and Hognestad (1956), Hawkins *et al.* (1989) and Tian *et al.* (2008) on thirteen slab-column connections without using shear reinforcement, as shown in Fig. 6, are used to determine and validate the key stiffness and strength parameters for the grid model described previously. These tests were chosen because they were performed on large-scale specimens and the

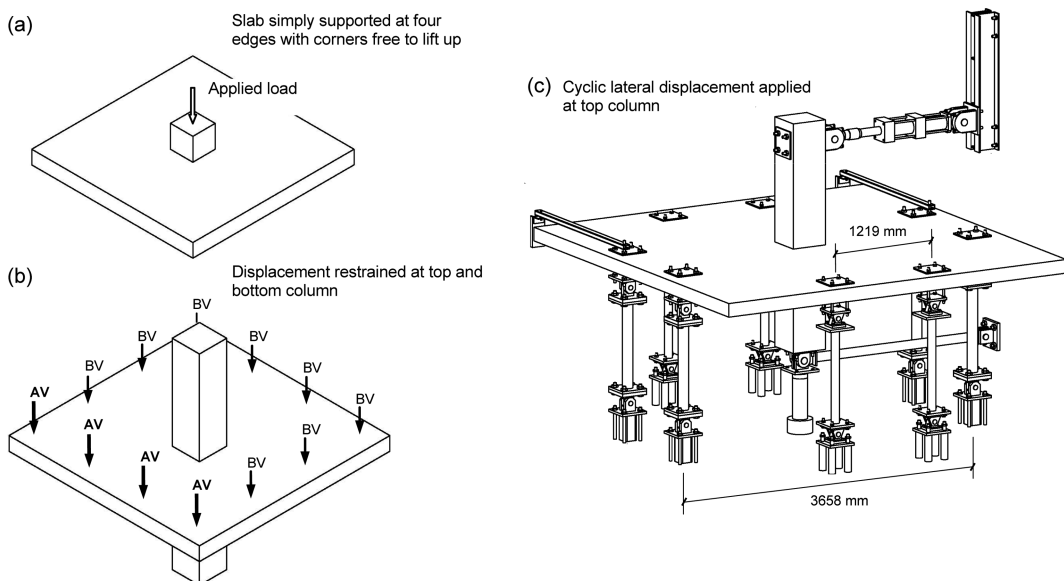


Fig. 6 Tests of slab-column connections: (a) concentric gravity loading (Elstner and Hognestad 1956), (b) uneven gravity loading (Hawkins *et al.* 1989) and (c) combined gravity and cyclic lateral loading (Tian *et al.* 2008)

Table 1 Specimen Properties

Test	Slab size (mm)	Column size (mm)	f'_c (MPa)	Tensile reinforcement		Loading
				f_y (MPa)	ρ_{avg} (%)	
A-1c	1829 × 1829 × 152	254	29.0	332	1.18	G
A-4	1829 × 1829 × 152	356	26.1	332	1.18	G
A-13	1829 × 1829 × 152	356	26.2	294	0.55	G
B-1	1829 × 1829 × 152	254	14.2	324	0.50	G
B-2	1829 × 1829 × 152	254	47.6	321	0.50	G
B-4	1829 × 1829 × 152	254	47.7	303	1.01	G
6AL	2134 × 2134 × 152	305	22.8	472	0.55	UG
9.6AL	2134 × 2134 × 152	305	29.0	415	0.89	UG
14AL	2134 × 2134 × 152	305	27.0	421	1.32	UG
6AH	2134 × 2134 × 152	305	31.4	472	0.55	UG
9.6AH	2134 × 2134 × 152	305	30.7	415	0.89	UG
14AH	2134 × 2134 × 152	305	30.3	421	1.32	UG
L0.5	4257 × 4267 × 152	406	25.6	441	0.49	LG

Note: f'_c = concrete cylinder compressive strength; G = concentric gravity load; UG = uneven gravity load causing unbalanced moment; LG = combined gravity load and cyclic lateral load

maximum coarse aggregate sizes needed to implement the punching failure criterion given in Eq. (5) were reported. Table 1 summarizes the geometry and material properties of these specimens. Three different types of loading were applied: (1) concentric gravity load, (2) unevenly distributed gravity load causing unbalanced moment and (3) combined gravity and cyclic lateral loading. In addition, the slab tensile reinforcement ratio in the column strip is one of the parameters controlling the behavior of a slab-column connection. Thus, specimens with different but practical slab reinforcement ratios are included.

The internal forces such as bending moment and torsion are not measurable even in the test of an isolated slab-column connection due to its static indeterminacy. Consequently, test data cannot be used to individually validate the modeling parameters. Concentric gravity loading (Fig. 6(a)) is the simplest loading condition, in which the concrete slab surrounding the column is primarily subjected to bending moment and shear and the effects of torsion on connection load-carrying capacity are insignificant. Therefore, the tests of specimens under concentric gravity loading are used to verify the definitions of the initial stiffness of flexure and torsion as well as the flexural strength for grid beams. The correction factor γ for post-cracking flexural stiffness and the torsional strength reduction factor λ are calibrated by one of these tests and verified by the remaining ones. In order to further validate the suggested grid beam model including the previously defined failure criterion, the tests of slab-column connections under unbalanced moment caused by unevenly distributed gravity load (Fig. 6(b)) are simulated. Finally, a test of slab-column connection subjected to combined gravity and cyclic lateral loading (Fig. 6(c)) is used to calibrate the four parameters defining the hysteretic response of principal bending moment and torsion in grid beams.

The analyses are carried out using the finite-element analysis package OpenSees (Open System for Earthquake Engineering Simulation 2010). Consistent with the loading schemes in tests, displacement-driven analysis is performed on the specimens under concentric gravity loading and

combined gravity and cyclic lateral loading, whereas force-driven analysis is employed for simulating the specimens under uneven gravity loads. A specimen is loaded in the analysis up to failure detected by Eq. (5). The reported material properties of the specimens are used to define the sectional properties regarding strength and stiffness. The concrete Young’s modulus, concrete modulus of rupture and ultimate flexural capacity of grid beams are evaluated in accordance with ACI 318-11. The *Hysteretic Material* option available in OpenSees is used to implement the nonlinear material models for principal bending moment and torsion. All other actions such as shear and axial force are assumed to be linear elastic. The grid beams are then modeled using *Nonlinear Beam-Column Element* that can consider the spread of plasticity along an element. Five integration points are defined for each element and Gauss-Lobatto quadrature rule is employed for integration.

3.2 Slab-column connections under concentric gravity loading

Elstner and Hognestad (1956) conducted a series of tests (Fig. 6(a)) on slab-column connections subjected to concentric gravity loading. The slab was placed up-side-down in a test and simply supported at four edges while the corners were free to lift up. Downward vertical load simulating gravity loading effects was applied at the center column stub. Six tests (A-1c, A-4, A-13, B-1, B-2 and B-4) are simulated. These specimens had identical slab geometry but different concrete compressive strengths (14.2 to 47.7 MPa) and different slab tensile flexural reinforcement ratios (0.50 to 1.18%). In the analyses, the actual test boundary conditions are simulated and equal vertical displacements are simultaneously applied at the four nodes corresponding to the column corners. Bond-slip of flexural reinforcement in grid beams is considered using the model described previously together with a type of fiber-based zero-length section element available in OpenSees. A duplicate (slave) node, as shown in Fig. 7, is defined at slab-column interface for this purpose. The master and slave nodes are permitted only with relative rotation and axial displacement caused by bar slip at the zero-length section.

Compared with other specimens, the larger deformation of Specimen A-1c at first-yielding due to the higher flexural reinforcement ratio enables a convenient examination of bond-slip effect. $\gamma=1$

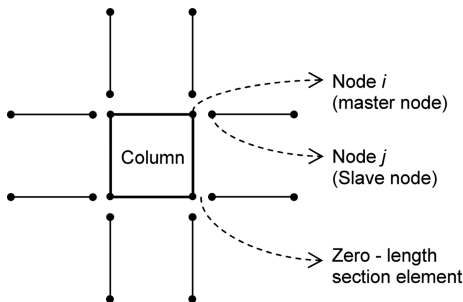


Fig. 7 Zero-length section element for simulating bond-slip

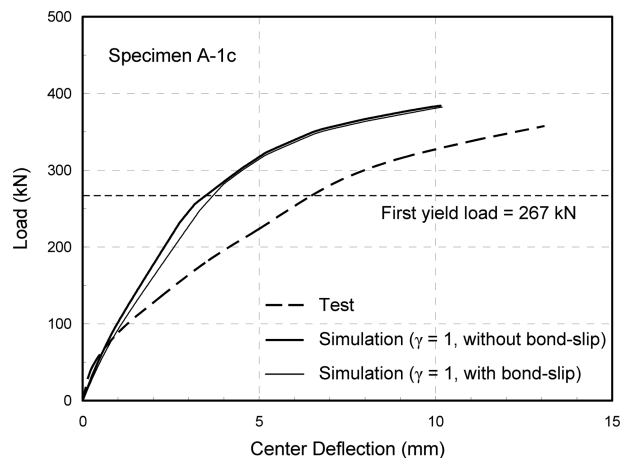


Fig. 8 Effects of bond-slip on connection stiffness (Specimen A-1c)

(without considering post-cracking stiffness reduction) is used first in Eq. (2) to define yield curvature. Fig. 8 compares the calculated load versus slab center deflection response with test result for this specimen. The inclusion of bond-slip of slab reinforcement in the modeling does not cause significant behavioral difference, as shown in Fig. 8. Specifically, the center deflection is about 10% higher than that without considering bond-slip prior to the first yielding. Additionally, bond-slip accounts for only a fraction of the notable difference between the calculated and measured deflections. The less significant effects of bond-slip than those in beams or columns can be explained by the lower flexural stiffness of slab, the smaller diameter of reinforcing bars normally used in slabs, and the continuity of slab surrounding column that restrains its rotation about slab-column interface. Because the effects of bond-slip on the deformation of slab-column connections are not decisive, bond-slip is not considered in the rest simulations.

To reduce the overestimated pre-yielding stiffness caused by using $\gamma=1$, different values of γ are applied to Specimen A-1c. The value of torsional strength reduction factor λ is also calibrated from this test. It is found that, as shown in Fig. 9(a), the use of $\gamma=2.5$ and $\lambda=0.8$ results in a good agreement between the predicted and measured load-deformation response for A-1c. The appropriateness of these values is then examined by simulating other tests. The results are shown in Figs. 9(b) through 9(f). The difference between the predicted and measured strength for all the specimens is less than 5%. Except for Specimen B-1, good agreement is achieved between the measured and predicted response in the initial loading stage, which validates the elastic stiffness definitions for flexure and torsion of grid beams. Relatively large difference in post-cracking stiffness still exists between the measured and predicted responses for Specimens B-1 and B-2. The discrepancy can be attributed to not only the simplifications made in the model but the inherent uncertainty involved in defining concrete tensile strength. Additionally, the analyses indicate that the definition of torsional strength affects the stiffness of slab-column connections mainly after first-yielding and has little influence in

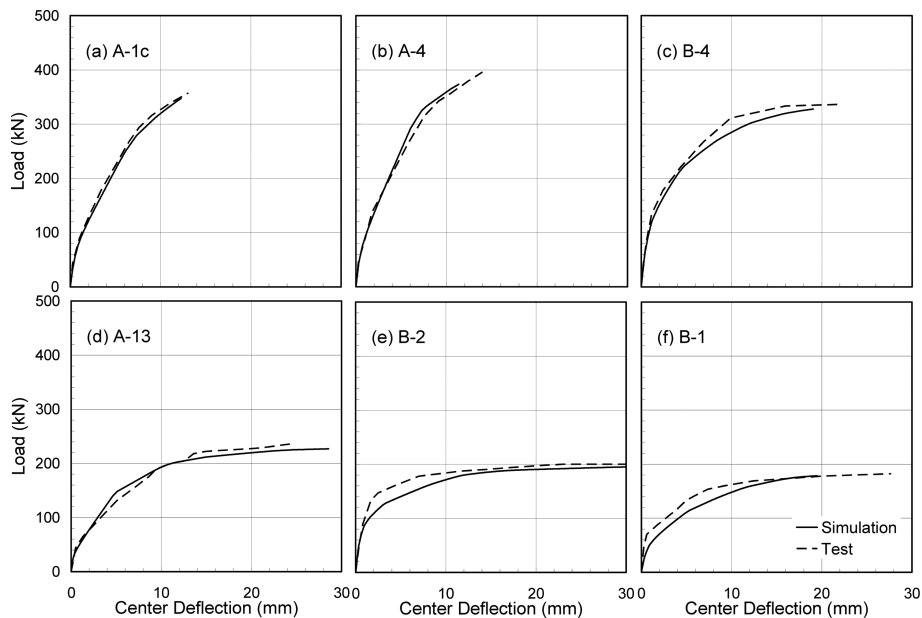


Fig. 9 Predicted versus measured load-deflection response for specimens under concentric gravity loading

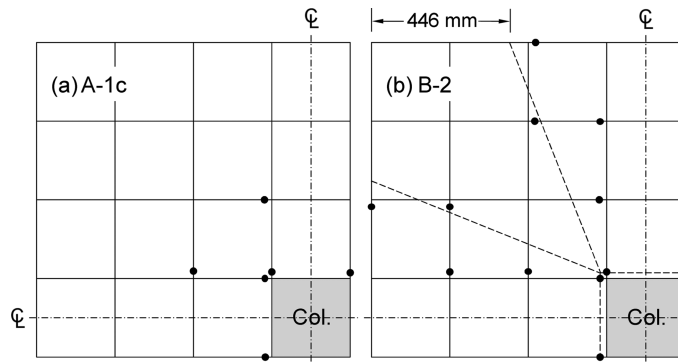


Fig. 10 Grid beam yield pattern and slab yield-line pattern for two specimens

their ultimate loading capacity.

The effectiveness of the suggested model is also examined by the yielding pattern of grid beams. Tests indicated that slab yielding always took place first at slab-column interface and, if the slab tensile reinforcement ratio was low, the yielding then spread until a general yielding occurred, leading to the formation of a collapse mechanism. Fig. 10(a) shows by circular dots the yielding of grid beams for a quarter of Specimen A-1c. Note that yielding identified from analysis is not limited at the beam ends but has extended along its length between the two nodes defining an element. It is seen that, consistent with the absence of a general yielding point in the load-deflection response, the yielding of grid beams for Specimen A-1c has not spread over the entire slab-column connection at its failure. In contrast, Specimen B-2 demonstrated an obvious general yielding in the measured load-deflection response. Fig. 10(b) compares the yield pattern of grid beams for this specimen with the yield-line pattern derived from Johansen's yield-line theory (Elstner and Hognestad 1956). The yield-lines, shown by the dashed lines, consist of those developed earlier at slab-column interface and those extending from column corners to the points located at slab edges. Fig. 10(b) indicates that the suggested grid beam model can also realistically capture the spread of slab yielding for slab-column connections.

3.3 Slab-column connections under uneven gravity loading

The proposed grid model is further validated by the tests of specimens under unbalanced moments. Six specimens with identical geometry tested by Hawkins *et al.* (1989) are considered. As shown in Fig. 6(b), the unbalanced moment was introduced by vertical loads unequally distributed around the slab perimeter. The level of unbalanced moment was represented by the ratio of unbalanced moment M to the total vertical shear V transferred between slab and column. For the tests with low M/V -ratio (130 mm), the vertical loads were maintained so that $AV=1.49BV$ throughout a test. For the tests with high M/V -ratio (584 mm), $AV=6.06BV$. Specimens 14AL, 9.6AL and 6AL were subjected to the lower level of unbalanced moment and had an average tensile reinforcement ratio of 1.32%, 0.89% and 0.55%, respectively. Specimens 14AH, 9.6AH and 6AH had corresponding reinforcement ratios but were subjected to the higher level of unbalanced moment. No matter the behaviors of these specimens can be treated as ductile or non-ductile in term of their overall load-deflection response, yielding of slab tensile reinforcement near column was observed in all the tests.

Because no column damage was observed in the tests, the columns are modeled in the analyses as

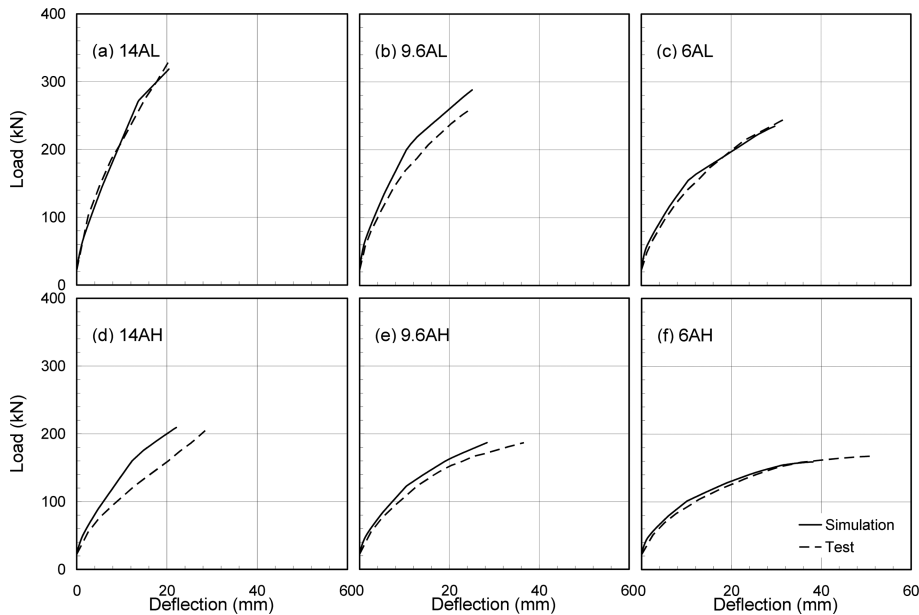


Fig. 11 Predicted versus measured load-deflection response for slab-column connections under uneven gravity loading

elastic elements. Loads simulating slab self-weight are applied first in the analysis. Unevenly distributed vertical loads are then applied until the shear and rotation of slab at the critical (heavily loaded) side of connection meet the punching failure criterion. Fig. 11 compares the measured and predicted load-deflection response for the six specimens. The load refers to the total gravity shear transferred from slab to column and deflection refers to that at the midpoint of a slab edge where the heavier loads (AV) shown in Fig. 6(b) are applied.

Good agreement is achieved between the predicted and measured load-deformation response for most specimens. The largest discrepancy occurs in Specimen 14AH. It appears that the stiffness of this specimen is remarkably overestimated. However, prior to reaching a load of 137 kN, the measured load-deformation response of this specimen was reported to be identical to that of Specimen 9.6AH. If 14AH could exhibit in the test higher post-cracking stiffness than 9.6AH due to the almost identical concrete strength and comparable loading condition but much higher reinforcement ratio, the predicted response would have been closer to the test result.

The yield patterns of these specimens are also examined. Fig. 12 shows the flexural yielding as well as torsional cracking in grid beams for half slab of each specimen. The heavier loads, AV, are applied at the right side of the slabs. It is seen that all the beams in Specimen 6AH oriented in the direction along which the unbalanced moment acts have yielded and, as expected, torsional cracking occurs in a slightly larger area surrounding the column due to the higher M/V -ratio in this specimen than 6AL.

The proposed grid model has also accurately captured the loading capacity of the specimens. As shown in Fig. 11, the predicted failure load for Specimens 9.6AH is 12% higher than the measure failure load, but the difference is less than 5% for all other tests. In addition to flexure, both shear and torsion participate in resisting unbalanced moment at slab-column connections. Thus, the accuracy obtained can be attributed to the properly defined torsional strength and failure criterion.

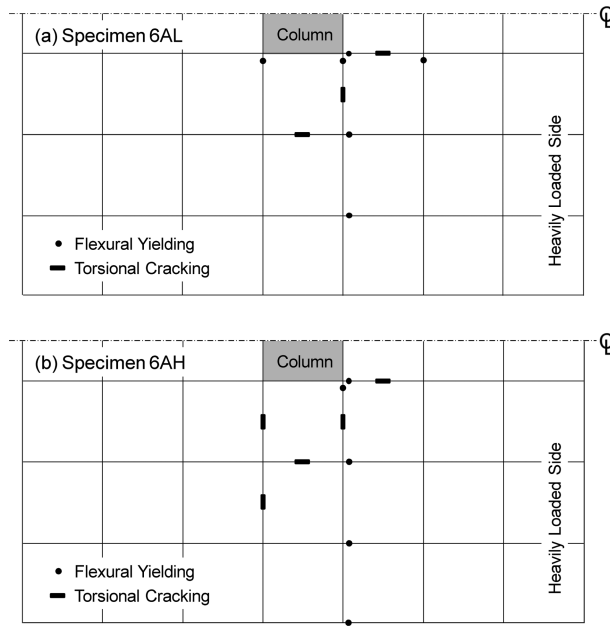


Fig. 12 Yield pattern in grid beams for specimens under unbalanced moment: (a) 6AL and (b) 6AH

Table 2 Calculated internal forces

Test	M_{ub} (kN·m)	M_{side} (kN·m)	M_T (kN·m)	M_{side}/M_{ub}	M_T/M_{ub}	V_1 (kN)	V_{ACI} (kN)
(1)	(2)	(3)	(4)	(5)	(6)	(7)	(8)
6AH	80.4	36.2	21.1	0.45	0.26	71.8	101.5
6AL	28.4	18.6	9.7	0.66	0.34	72.6	86.5
9.6AH	103.3	40.0	21.1	0.39	0.20	87.6	100.3
9.6AL	33.9	16.9	7.8	0.50	0.23	90.5	97.5
14AL	38.4	10.5	4.8	0.27	0.12	103.0	94.1

Note that the punching failure criterion suggested by Muttoni (2008) was developed based on the tests of slab-column connection under concentric gravity loading only. The numerical simulations conducted herein indicate that this punching failure condition can also be applied to the slab-column connections subjected to more complex loading conditions. Because the grid beam model closely simulates the response of Specimens 6AH, 6AL, 9.6AH, 9.6AL and 14AL, their internal forces at failure that cannot be measured in the tests are examined by analysis results. Table 2 gives the externally applied unbalanced moment (M_{ub}), the total unbalanced moment resisted by the grid beams at two side faces (M_{side}), and the total resistance provided by torsion in grid beams ($M_T = 2(T_1 + T_2)$ with T_1 and T_2 shown in Fig. 2) at two side faces. As indicated by the ratios of M_{side} to M_{ub} shown in Column (5), the side faces resist a significant portion of the total unbalanced moment. However, only about half of this resistance is provided by torsion developed in the grid beams, which permits the model for torsional strength in a simplified manner without significantly sacrificing accuracy. Table 2 also compares the total shear at the back face of connections

determined from analyses at failure, V_1 , and the nominal shear strength at this location determined from ACI 318-11 (2011), V_{ACI} . The comparison indicates the ACI code approach overestimates the shear strength of all the connections with slab reinforcement ratios less than 1%.

3.4 Slab-column connections under gravity and cyclic lateral loading

The test of an isolated slab-column specimen L0.5 (Tian *et al.* 2008) is simulated using the suggested grid beam model to calibrate the parameters p_x , p_y , β and γ_1 defining the hysteretic model shown in Fig. 4. Fig. 6(c) shows the specimen and test setup. The slab average top reinforcement ratio was 0.49% in the column strip and 0.25% elsewhere. In the test, the bottom end of the column was restrained from lateral displacement but vertical displacement was permitted. An upward vertical load of 105 kN was first applied to the specimen through a hydraulic jack placed underneath the column. This load simulated the shear transferred between slab and column due to service level gravity load. Cyclic lateral displacements simulating seismic effects were then applied at the top column through an actuator, while the previously applied vertical load was maintained constant. Three loading cycles were applied at each lateral drift level. Punching failure occurred in the tests soon after 2.0% drift was achieved.

Simulation of the test is performed first by applying loads corresponding to slab self-weight and the upward vertical load at slab center. Cyclic lateral displacement is then applied until three loading cycles at 2.0% drift is completed. The four parameters leading to the best fit with the measured lateral load-drift response are calibrated as $p_x=0.75$, $p_y=0.30$, $\beta=0.48$ and $\gamma_1=0.09$. The calculated and measured cyclic lateral load-drift responses are shown in Fig. 13. Note that, there was a drop of load at the end of each lateral drift during the test (as shown in Fig. 13). This was caused by force relaxation in the actuator when the drift was hold so that slab damage could be examined and marked.

Likely due to the single unloading stiffness adopted in the model shown in Fig. 4, it is difficult to achieve excellent agreement between the simulated response and test results. Thus, the appropriateness of the calibrated parameters needs to be further examined. Under combined gravity and cyclic lateral loading, slab vertical deflection measured in the test increased as the damage to slab caused by lateral drifts was accumulated. In addition to the connection lateral load-displacement response, the

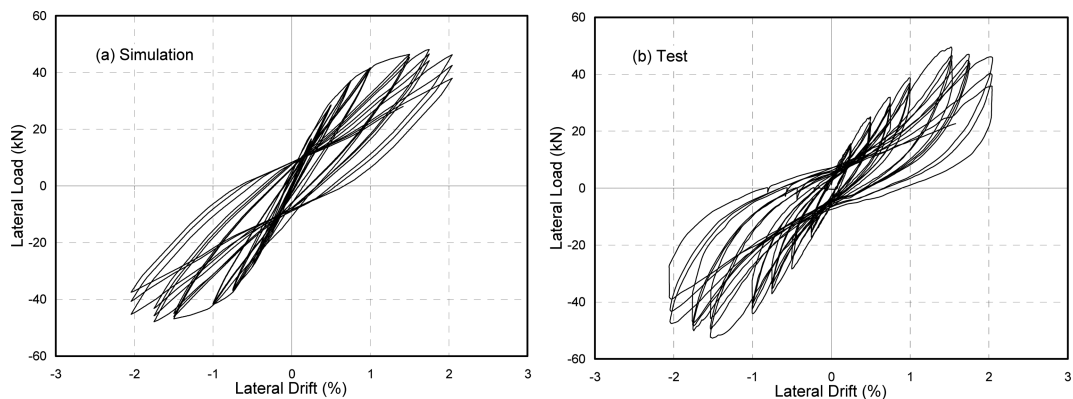


Fig. 13 Comparison of calculated versus measured hysteretic behavior

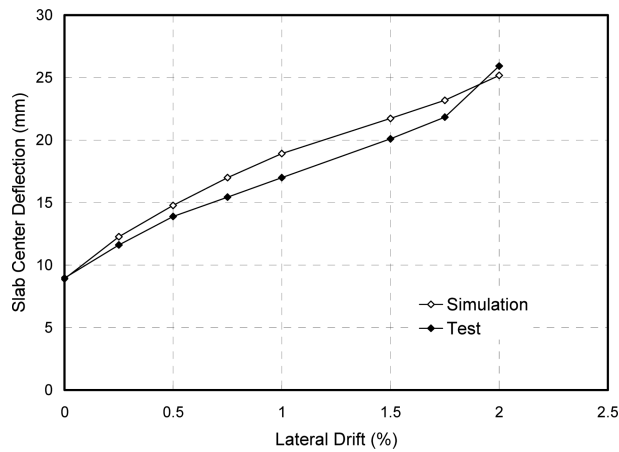


Fig. 14 Slab vertical deflection versus lateral drift

increased slab vertical deflection due to increased lateral deformation is an indicator of slab stiffness degradation. Fig. 14 compares the calculated and measured results (Tian 2007) for the lateral drift versus vertical displacement response. The slab center deflection in this figure refers to that determined when the specimen has been unloaded after the three loading cycles at a drift level have been completed. As shown in this figure, using the calibrated parameters for p_x , p_y , β and γ_1 , good agreement can also be reached between predictions and test results. Additionally, the slab vertical deflection right after applying vertical loads (before any lateral load is applied) is calculated as 8.90 mm, whereas this deflection was measured in the test as 8.96 mm. Because slab cracking due to the initially applied gravity loading is identified in both analysis and test, the almost identical slab vertical deflections validate once again the definition of post-cracking flexural stiffness of grid beams.

The applicability of Eq. (5) to flat-plates subjected to cyclic loading is also examined. Specimen L0.5 survived 2% lateral drift in the test but was unable to reach the next level of lateral deformation. At 2% drift, the peak shear and slab rotation demand at the back face of connection are determined from analyses as 72.8 kN and 0.016 rad. According to Eq. (5), the specimen should survive this drift level because the slab rotational capacity is evaluated as 0.021 rad. Compared with monotonic loading, cyclic loading causes more material damage and thus may reduce the connection deformation capacity. However, it appears that Eq. (5) has the potential of estimating an upper bound deformation capacity for a slab-column connection under reversed cyclic loading.

4. Conclusions

This study investigates a type of grid beam model used for simulating the nonlinear behavior of reinforced concrete flat-plate structures. The tests of twelve large-scale isolated slab-column connection specimens are used to calibrate and validate the model for monotonic loading. The test of a connection subjected to combined gravity and cyclic lateral loading is used to calibrate the parameters defining a hysteretic behavioral model. The use of the proposed grid beam model and the punching failure criterion suggested by Muttoni can accurately predict the loading capacity of

slab-column connections under monotonic loading. The model can also closely capture the overall nonlinear response of slab-column connections as well as slab yielding pattern. Additionally, the numerical simulations indicate that, under monotonic loading, bond-slip of slab flexural reinforcement likely cause insignificant effects on connection deformation and thus can be neglected. For cyclic loading conditions, the effects of bond slip may be more obvious and thus considered for future research. The proposed model is developed based on the tests of slabs framing with square columns. Further study is needed to verify the effectiveness of this model for connections with rectangular columns or structural walls.

References

- ACI Committee 318 (2011), *Building code requirements for structural concrete (ACI 318-11) and commentary*, American Concrete Institute, Farmington Hills, Michigan, USA.
- Akiyama, H. and Hawkins, N.M. (1984), *Response of flat plate concrete structures to seismic and wind forces*, Structures and Mechanics Report SM84-1, Department of Civil Engineering, University of Washington, Seattle, 320.
- Coronelli, D. (2010), "Grid model for flat-slab structures", *ACI Struct. J.*, **107**(6), 645-653.
- Dovich, L.M. and Wight, J.K. (2005), "Effective slab width model for seismic analysis of flat slab frames", *ACI Struct. J.*, **102**(6), 868-875.
- Elstner, R.C. and Hognestad, E. (1956), "Shearing strength of reinforced concrete slabs", *ACI J. Proc.*, **53**(1), 29-58.
- Elwood, K.J. (2002), *Shake table tests and analytical studies on the gravity load collapse of reinforced concrete frames*, Ph.D. thesis, University of California, Berkeley, California.
- FIB Task Group on Bond Models (2000), *Bond of reinforcement in concrete*, Bulletin 10, Lausanne, Switzerland, 427.
- Guandalini, S., Burdet, O.L. and Muttoni, A. (2009), "Punching tests of slabs with low reinforcement ratios", *ACI Struct. J.*, **106**(1), 87-95.
- Hawkins, N.M., Bao, A. and Yamazaki, J. (1989), "Moment transfer from concrete slabs to columns", *ACI Struct. J.*, **86**(6), 705-716.
- Hsu, T.T.C. (1968), "Torsion of structural concrete-interaction surface for combined torsion, shear, and bending in beams without stirrups", *ACI J.*, **65**(1), 51-60.
- Kang, T.H.K., Wallace, J.W. and Elwood, K.J. (2009), "Nonlinear modeling of flat-plate systems", *J. Struct. Eng.-ASCE*, **135**(2), 147-158.
- Kanoh, Y. and Yoshizaki, S. (1979), "Strength of slab-column connections transferring shear and moment", *ACI J.*, **76**(3), 461-478.
- Luo, Y.H., Durrani, A.J. and Conte, J.P. (1994), "Equivalent frame analysis of flat plate buildings for seismic loading", *J. Struct. Eng.-ASCE*, **120**(7), 2137-2155.
- Morrison, D.G., Hirasawa, A.M. and Sozen, M.A. (1983), "Lateral-load tests of R/C slab-column connections", *J. Struct. Eng.-ASCE*, **109**(11), 2698-2714.
- Muttoni, A. (2008), "Punching shear strength of reinforced concrete slabs without transverse reinforcement", *ACI Struct. J.*, **105**(4), 440-450.
- OpenSees (2010), *Open system for earthquake engineering simulation*, <http://opensees.berkeley.edu>.
- Park, P. and Gamble, W.L. (2000), *Reinforced concrete slabs*, 2nd ed., John Wiley & Sons.
- Robertson, I.N. (1997), "Analysis of flat slab structures subjected to combined lateral and gravity loads", *ACI Struct. J.*, **94**(6), 723-729.
- Sheu, M.S. and Hawkins, N.M. (1980), "Grid model for predicting the monotonic and hysteretic behavior of slab-column connections transferring moments", ACI SP 63-04, 79-111.
- Tian, Y. (2007), *Behavior and modeling of reinforced concrete slab-column connections*, Ph.D. thesis, University of Texas at Austin, Austin, Texas.

- Tian, Y., Jirsa, J.O., Bayrak, O. Widiyanto and Argudo, J.F. (2008), "Behavior of slab-column connections under different loading histories", *ACI Struct. J.*, **105**(5), 561-569.
- Tian, Y., Jirsa, J.O. and Bayrak, O. (2009), "Nonlinear modeling of slab-column connections under cyclic loading", *ACI Struct. J.*, **106**(1), 30-38.
- Yettram, A. and Husain, H.M. (1965), "Grid-framework method for plates in flexure", *J. Eng. Mech. Div. ASCE*, **63**(3), 53-64.
- Zhao, J. and Sritharan, S. (2007), "Modeling of strain penetration effects in fiber-based analysis of reinforced concrete structures", *ACI Struct. J.*, **104**(2), 133-141.

CC